Weierstraß-Institut
für Angewandte Analysis und Stochastik

im Forschungsverbund Berlin e.V.

Optimal Control of Robot Guided Laser Material Treatment

Dietmar Hömberg[1], Andreas Steinbrecher[2], Tatjana Stykel[2]

submitted: December 22, 2009

[1] Weierstrass Institute for Applied Analysis and Stochastics Mohrenstrasse 39 10117 Berlin Germany E-mail: hoemberg@wias-berlin.de	[2] Technische Universität Berlin Institut für Mathematik, MA 4-5 Strasse des 17. Juni 136 10623 Berlin Germany E-mail: steinbrecher@math.tu-berlin.de stykel@math.tu-berlin.de

W I A S

Abstract

In this paper, we consider the optimal control problem for robot guided laser material treatments, where the discrete multibody system model of a robot is coupled with a PDE model of the laser treatment. We present several optimization approaches of such an optimal control problem and discuss their properties in view of a robust and suitable numerical solution. We illustrate these approaches in an application to the surface hardening of steel.

1   Introduction

Laser material treatments such as hardening or welding have become a basic part of the process chain for sophisticated metal workpieces. They allow for precise process control with reproducible results. Mounted on industrial robots, laser treatment devices become increasingly important in automated manufacturing, especially in automotive industry.

For the employment of single robots numerous papers are available, considering issues like path-planning, control, collision detection, etc., e.g., see [3, 13, 14, 23, 22]. However, typically the specific task the robot has to perform is disregarded. In the case of laser treatments up to now, it is always assumed that the track along which the laser light impinges on the workpiece surface is precisely known. In [11, 12] optimal control problems for laser surface treatments have been studied, where the laser track on the surface is a prescribed function.

However, especially in the case of curved workpiece boundaries, the real movement of the robot tool center point and, thus, the laser track as well as the laser velocity may differ considerably from the desired one. In particular, depending on the workpiece geometry, the desired laser track cannot sometimes be realized. On the other hand, the most natural criterion to decide, whether the employment of a robot has been successful, is not the tracking of a prescribed path, but the question whether the robot has achieved its production goal.

In this paper, we consider the optimal control problem for robot guided laser material treatments, accounting for robot motion planing as well as for the thermal effects induced by the laser. To this end, the discrete multibody system model of a robot is coupled with a PDE model of the laser treatment. We present several optimization approaches of such an optimal control problem and discuss their properties in view of a robust and suitable numerical solution. We illustrate these approaches in an application to the surface hardening of steel.

The paper is organized as follows. In Section 2, the mathematical model for the

coupled robot and laser treatment is derived. Section 3 describes three different optimization approaches for the optimal control problem. In each case, the optimality system is derived in a formal way using the Lagrangian framework. Numerical results are also presented for a gradient based method. Section 4 is devoted to a comparison of the different approaches.

2 The mathematical model

Typically, the goal of the laser treatment is to achieve a certain change in material properties of the *workpiece* $\Omega \subset \mathbb{R}^3$ along a given path on its surface Γ within a given time interval $\mathbb{I} = [0, T]$. The path is defined by a space curve

$$\gamma = \begin{bmatrix} \gamma_1 & \gamma_2 & \gamma_3 \end{bmatrix}^T : [0,1] \to \Gamma \subset \mathbb{R}^3. \tag{1}$$

The curve γ will be called the *target curve*. Another important curve is the *laser acting curve*

$$l = \begin{bmatrix} l_1 & l_2 & l_3 \end{bmatrix}^T : \mathbb{I} \to \Gamma \subset \mathbb{R}^3, \tag{2}$$

which describes the real position of the laser on the workpiece surface Γ. In general, one cannot expect that laser curve l and target curve γ coincide.

A part of the laser light is absorbed volumetrically in a boundary layer of the workpiece leading to a rise in temperature in this region. The changing temperature triggers either solid - solid or solid - liquid - solid phase transitions in the workpiece, which are responsible for the desired hardening, welding, cutting or remelting effect. In this paper, we neglect the effect of possible phase transitions and refer to [10, 12] instead.

The production goal is simply to achieve a *desired temperature profile* θ^* inside a bounded *target region* given as a flat cylinder sliding under the surface Γ. This target region is represented by a weight function ω moving along the target curve γ with $\gamma(\xi) \in \Gamma$ for all $\xi \in [0,1]$, see Figure 1. The parameter $\xi = \xi(t)$ depends on the time $t \in \mathbb{I}$ and determines the movement of the target region ω. To achieve the desired phase transition along the curve, the laser should not fall below a certain exposure time somewhere along the curve. We choose $\xi(t) = t/T$. To avoid technicalities, we assume in the sequel that the part of the boundary impinged by the laser lies in the plane $x_3 = 0$. In this case ω can be described as

$$\omega(x,t) = \begin{cases} 1 & \text{if } \sqrt{(\gamma_1(\xi(t)) - x_1)^2 + (\gamma_2(\xi(t)) - x_2)^2} \leq r \text{ and } |x_3| \leq h, \\ 0 & \text{else}, \end{cases}$$

with given target region height $h = 0.05\,\text{cm}$ and target region radius $r = 0.2\,\text{cm}$.

In the following, we consider several approaches for the optimization problem to minimize the *objective functional J* subject to the heat conduction process within the workpiece influenced by the robot guided laser treatment. The objective functional J is defined as
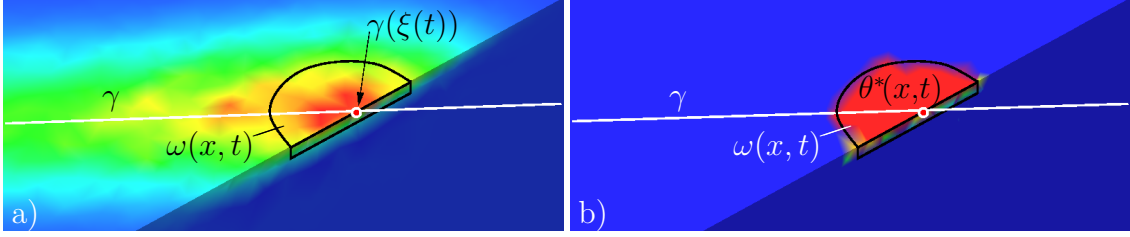
$$J = J_\theta + J_R, \tag{3}$$

2

Figure 1: a) target curve γ and target region ω, b) target region ω and desired temperature profile θ^*

where

$$J_\theta = \frac{1}{2} \int_0^T \int_\Omega \omega(x,t)(\theta(x,t) - \theta^*(x,t))^2 \mathrm{d}x \ \mathrm{d}t \tag{4}$$

evaluates the temperature profile θ within the moving target region ω, and J_R contains some regularization and/or penalty terms depending on the respective approach.

The temperature distribution θ is governed by the heat equation

$$\begin{aligned}
\rho c \tfrac{\partial}{\partial t}\theta(x,t) - \kappa \Delta\theta(x,t) &= F(x,l,u_l) && \text{on} && \Omega \times \mathbb{I}, \\
\theta(x,0) &= \theta_0 && \text{on} && \Omega, \\
\tfrac{\partial}{\partial \nu}\theta(x,t) &= 0 && \text{on} && \Gamma \times \mathbb{I},
\end{aligned} \tag{5}$$

where ρ denotes the mass density, c denotes the specific heat, and κ denotes the heat conductivity. Here, we use $\rho c = 7.4\frac{\text{J}}{\text{cm}^3\,\text{K}}$ and $\kappa = 0.3\frac{\text{J}}{\text{s cm K}}$ corresponding to a low-alloyed carbon steel. and assume that the *laser power* u_l is volumetrically absorbed by the workpiece Ω. As mentioned before, we restrict our investigations to workpieces, where the laser treated surface is flat and lies parallel to the plane $z = 0$. Then the laser power absorption of a CO_2-laser can be modeled by the energy distribution

$$E(x,l) = \frac{a}{\pi D^2} e^{-\frac{(x_1 - l_2(t))^2 + (x_2 - l_2(t))^2}{D^2}} e^{a(x_3 - l_3(t))} \tag{6}$$

in the neighborhood of the laser acting point $l(t) = [l_1(t), l_2(t), l_3(t)]^T \in \Gamma$. Here, $a = 60.0\frac{1}{\text{cm}}$ and $D = 0.47\,\text{cm}$ are the absorptivity and the laser diameter, respectively. The inhomogeneity F in the heat equation (5) is given by

$$F(x,l,u_l) = u_l E(x,l), \tag{7}$$

where the laser power $u_l \in \mathcal{U}_{ad}^{u_l}$ is the *laser control* and $\mathcal{U}_{ad}^{u_l} = L^2(\mathbb{I})$ is the admissible set. For more details on modeling the laser treatment and simulation methods, we refer to [7, 12].

As a basis for the simulation of the dynamical behavior of a robot, the equations of motion provide a useful tool for modeling the relevant dynamical properties, e.g., [1, 16, 20]. They can be generated in a systematic way by multibody formalism based on the principles of classical mechanics [5, 15, 18, 19]. Let the vector p

3

consist of arbitrary nonredundant coordinates (joint angles, joint displacements), which describe the *positions* of all relevant bodies involved in the robot. Moreover, let the derivative $\dot{p} = dp/dt$ of the position variables with respect to t denotes the generalized velocity of the robot. From the Euler equations [4, 6, 17], one obtains the equations of motion in the state space form

$$M(p)\ddot{p} = \tilde{f}(p, \dot{p}, t) + \tilde{B}u_r, \qquad p(0) = p_0, \ \dot{p}(0) = v_0, \tag{8}$$

where M is the mass matrix, the function $\tilde{f}(p, \dot{p}, t)$ describes gravitational forces and gyroscopic forces, $u_r \in \mathcal{U}_{ad}^{u_r} = (L^2(\mathbb{I}))^{n_{u_r}}$ is the robot control, n_{u_r} the number of robot controls, and $\tilde{B}u_r$ models the external forces. Furthermore, p_0 and v_0 are given initial position and velocity vectors.

Since we consider serial robots only, the matrix M is nonsingular. In this case, the second-order equations of motion (8) can be brought into the form

$$\ddot{p} = f(p, \dot{p}, t) + Bu_r, \qquad p(0) = p_0, \ \dot{p}(0) = v_0 \tag{9}$$

with $f = M^{-1}\tilde{f}$ and $B = M^{-1}\tilde{B}$. Introducing the velocity variable v, we obtain the first-order equations of motion

$$\begin{aligned} \dot{p} &= v, & p(0) &= p_0, \\ \dot{v} &= f(p, v, t) + Bu_r, & v(0) &= v_0, \end{aligned} \tag{10}$$

which can also be written as

$$\dot{q} = k(q, u_r, t), \qquad q(0) = q_0 \tag{11}$$

with $q = [\, p^T, \ v^T \,]^T$ and $q_0 = [\, p_0^T, \ v_0^T \,]^T$. From the numerical analysis point of view, there exists a large collection of efficient and robust solvers for the numerical integration of the equations of motion (9), (10), or (11), see [2, 8, 9, 21].

Summarizing, we have the following optimal control problem: minimize the cost functional J as in (3) subject to the equations of motion (9), (10), or (11) and the heat equation (5).

3 Optimization Approaches and Numerical Results

3.1 Preliminaries

In this section, we discuss three different approaches for the optimal control of robot guided heat treatments. These optimization approaches are

- laser power and Laser Position Optimization (LPO), see Section 3.2,

- laser power and Laser Track Optimization (LTO), see Section 3.3,

- laser power and Robot Control Optimization (RCO), see Section 3.4.

In all these approaches, the target curve γ is prescribed. In LPO, the laser track is restricted to the target curve and controls are the laser power and the actual position of the heat source on the track. In LTO, both laser power and track act as controls, while in RCO, the laser power and the torques in the robot joints are considered as controls. For completeness, in the appendix, we also discuss laser power and Robot Motion Optimization (RMO), where the laser power and the position vector p of the robot are used as controls. However, this approach turns out to be numerically infeasible.

The optimization is done using a gradient based method. By use of the Lagrange approach, the first-order optimality conditions are derived formally and the gradient functions with respect to the used control variables are characterized in terms of the adjoint variables. The gradient based method is implemented with alternating line search, where the line search alternately uses the gradient function with respect to the robot control and with respect to the laser control.

For spatial discretization the numerical solution of the heat equation (5) and the corresponding adjoint equation via the finite element method (FEM), we use FEM tools and grid generator provided by `pdelib`[1]. The semidiscretized PDE equations are solved then in time using the implicit Euler method, while the equations of motion (11) for the robot is simulated using the classical Runge-Kutta method. The right-hand side k in (11) is provided by INVISION[2]. The time interval $\mathbb{I} = [0, T]$ with $T = 5\,\mathrm{s}$ was discretized with equidistant time steps $t_i = ih$, where $h = 0.01$ and $i = 0, ..., 500$.

We will present the numerical results and discuss the properties of all approaches for two different scenarios described below. In both scenarios, the workpiece Ω is defined as a cuboid with width (x_1-direction) of $2\,\mathrm{cm}$, length (x_2-direction) of $15\,\mathrm{cm}$, and height (x_3-direction) of 1cm, see Figure 2. Furthermore, this workpiece contains a hole also in form of a cuboid of size $2\,\mathrm{cm} \times 5\,\mathrm{cm} \times 0.8\,\mathrm{cm}$ located in the center of the workpiece. The numerical experiments were done on an Intel(R) Xeon(R) CPU 5160 with 3.00GHz. The initial temperature distribution is $\theta_0 = 300\,\mathrm{K}$ and the initial state of the robot is chosen such that the laser points into the starting point of the target curve, i.e., $l(0) = \gamma(0)$. The production goal is to achieve a desired temperature $\theta^* = 1200\,\mathrm{K}$ inside the target region ω moving along the respective target curve γ.

Scenario I: Here, the target curve is given by

$$\gamma_I(\xi) = \begin{bmatrix} \cos(\xi) & 15\xi & 0 \end{bmatrix}^T \tag{12}$$

---

[1] `pdelib` is a collection of software components for solving PDEs. In particular finite volume and finite element methods are supported. `pdelib` is developed by Weierstrass Institute for Applied Analysis and Stochastics (WIAS) in Berlin.

[2] INVISION is a software package for the real-time simulation of manufacturing plants developed and supported by Rücker EKS. Its data base includes all relevant industrial robots currently used in industry.
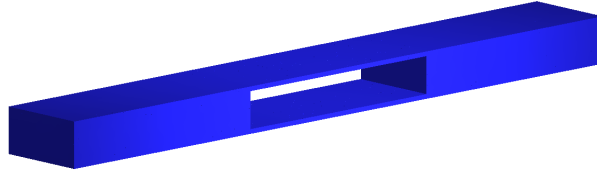
Figure 2: Treated workpiece.

with $\xi = \xi(t) = t/T$ and $t \in \mathbb{I}$, see Figure 3. The spatial discretization of the workpiece using FEM with linear finite elements is done with 47384 nodes, where the FEM grid is refined along the target curve γ_I as shown in Figure 5. ◁
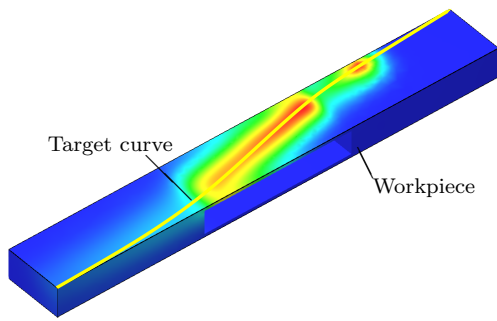
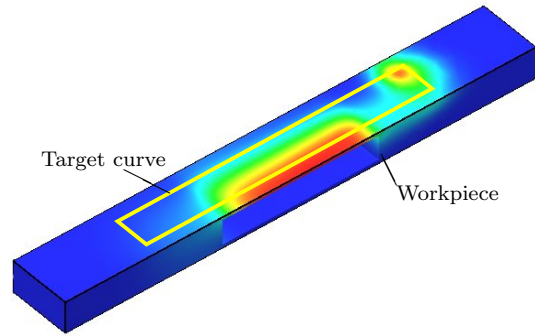

Figure 3: Target curve for Scenario I.
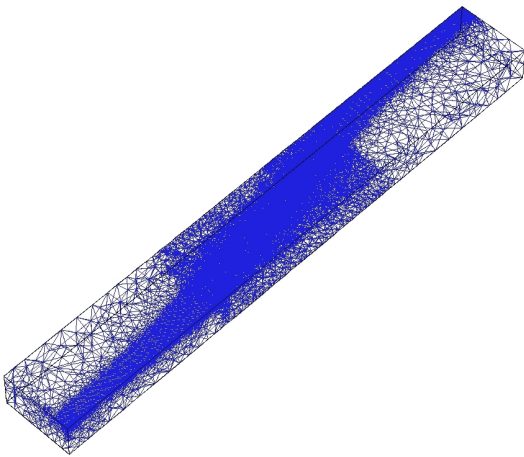

Figure 4: Target curve for Scenario II.
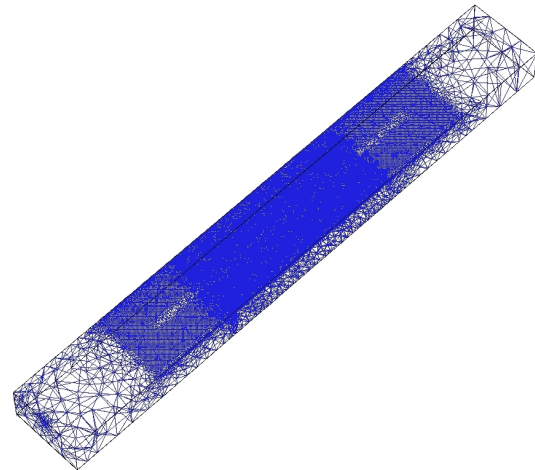

Figure 5: FEM grid for Scenario I (47384 nodes).

Figure 6: FEM grid for Scenario II (49125 nodes).

6

Scenario Ⅱ: The target curve is

$$\gamma_{Ⅱ}(\xi) = \begin{cases} \begin{bmatrix} 0.5 & 3+20\xi & 0 \end{bmatrix}^T & \text{for } \xi \in [0.00, 0.45), \\ \begin{bmatrix} 0.5-20\xi & 17 & 0 \end{bmatrix}^T & \text{for } \xi \in [0.45, 0.55), \\ \begin{bmatrix} -0.5 & 17-20\xi & 0 \end{bmatrix}^T & \text{for } \xi \in [0.55, 0.95), \\ \begin{bmatrix} -0.5+20\xi & 3 & 0 \end{bmatrix}^T & \text{for } \xi \in [0.95, 1.00] \end{cases} \tag{13}$$

with $\xi = \xi(t) = t/T$, see Figure 4. Note that the target curve $\gamma_{Ⅱ}$ is nonsmooth in contrast to the target curve γ_I. The spatial discretization of the workpiece using linear finite elements is done with 49125 nodes, see Figure 6. ◁

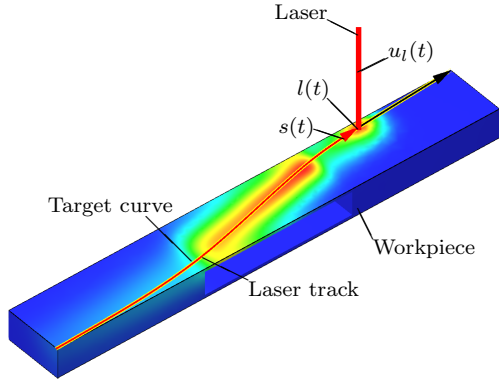## 3.2 Laser Power and Laser Position Optimization
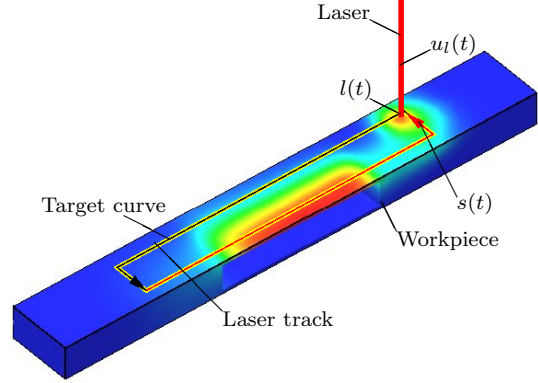

Figure 7: Laser position optimization of Scenario I

Figure 8: Laser position optimization of Scenario Ⅱ

In this approach, the laser acting curve l is restricted to the target curve γ such that $l(t) = \gamma(s(t))$, where $s : \mathbb{I} \to [0, 1]$ is the *laser position* function. Furthermore, the laser guiding robot is neglected and the equations of motion (11) for the robot are removed from the model.

For $t \in \mathbb{I}$, we aim to find an optimal laser power $u_l \in \mathcal{U}_{ad}^{u_l}$ and an optimal laser position $s \in \mathcal{U}_{ad}^s$ that minimize

$$J(u_l, s) = J_\theta + J_R = J_\theta + \frac{\alpha}{2} \int_0^T u_l(t)^2 \, \mathrm{d}t + \frac{\beta}{2} \int_0^T \ddot{s}(t)^2 \, \mathrm{d}t \tag{14}$$

subject to the heat equation (5). In addition to J_θ given in (4), the objective functional J contains two regularization terms penalizing high power and strong acceleration of the laser with weights α and β, respectively. In particular, the penalty term β causes a smoothing of the laser movement within the target curve γ such that oscillations are reduced by increasing parameter β. This improves the

7

realizability of the laser track by the robot. The admissible set $\mathcal{U}_{ad}^s$ is chosen here as

$$\mathcal{U}_{ad}^s = \{\, s \in C^4(\mathbb{I}, \mathbb{R}) \quad | \quad \ddot{s}(0) = \ddot{s}(T) = 0, \;\; s^{(3)}(0) = s^{(3)}(T) = 0 \,\} \qquad (15)$$

Another possible choice for $\mathcal{U}_{ad}^s$ could have been to prescribe $s(t)$ and $\dot{s}(t)$ at $t = 0$ and $t = T$. As shown in [12] the hot-spot, which should be in the target region lags behind the laser acting point. However, this distance between the laser acting point and the hot-spot depends on the current laser velocity und laser power and is unknown in advance. Therefore, we have chosen not to restrict s and $\dot{s}$ at the beginning and the end of $\mathbb{I}$ by the admissible set $\mathcal{U}_{ad}^s$.

With the Lagrange multipliers μ_θ, the Lagrange function is given by

$$
\begin{aligned}
L(\theta, s, u_l, \mu_\theta) \;=\; & \frac{1}{2} \int_0^T \int_\Omega \omega(\theta - \theta^*)^2 \, \mathrm{d}x \, \mathrm{d}t + \frac{\alpha}{2} \int_0^T u_l^2 \, \mathrm{d}t + \frac{\beta}{2} \int_0^T \ddot{s}^2 \, \mathrm{d}t \\
& - \int_0^T \int_\Omega \mu_\theta \big(\rho c \tfrac{\partial}{\partial t}\theta - \kappa \Delta\theta - F\big) \, \mathrm{d}x \, \mathrm{d}t - \int_0^T \int_\Gamma \mu_\theta \tfrac{\partial}{\partial\nu}\theta \, \mathrm{d}x \, \mathrm{d}t.
\end{aligned}
$$

Necessary condition for a stationary point $(\hat{\theta}, \hat{s}, \hat{u}_l)$ to be optimal is that the relations

$$
\begin{aligned}
\tfrac{\partial}{\partial\theta} L h_\theta = 0 && \text{on} \quad \Omega \times \mathbb{I}, && (16a) \\
h_\theta(x, 0) = 0 && \text{on} \quad \Omega, && (16b) \\
\tfrac{\partial}{\partial\nu} h_\theta(x, t) = 0 && \text{on} \quad \Gamma \times \mathbb{I}, && (16c)
\end{aligned}
$$

$$
\begin{aligned}
\tfrac{\partial}{\partial s} L(s - \hat{s}) \geq 0, && (16d) \\
\tfrac{\partial}{\partial u_l} L(u_l - \hat{u}_l) \geq 0 && (16e)
\end{aligned}
$$

are satisfied for all suitable test functions h_θ, for $s \in \mathcal{U}_{ad}^s$ and $u_l \in \mathcal{U}_{ad}^{u_l}$. We have

$$
\begin{aligned}
\tfrac{\partial}{\partial\theta} L h_\theta \;=\; & \int_0^T \int_\Omega \omega(\hat{\theta} - \theta^*) h_\theta \, \mathrm{d}x \, \mathrm{d}t - \rho c \int_0^T \int_\Omega \mu_\theta \tfrac{\partial}{\partial t} h_\theta \, \mathrm{d}x \, \mathrm{d}t \\
& + \kappa \int_0^T \int_\Omega \mu_\theta \Delta h_\theta \, \mathrm{d}x \, \mathrm{d}t - \int_0^T \int_\Gamma \mu_\theta \tfrac{\partial}{\partial\nu} h_\theta \, \mathrm{d}x \, \mathrm{d}t.
\end{aligned}
$$

Using integration by parts in space and time, we obtain that

$$
\begin{aligned}
\tfrac{\partial}{\partial\theta} L h_\theta \;=\; & \int_0^T \int_\Omega \big(\omega^2(\hat{\theta} - \theta^*) + \rho c \tfrac{\partial}{\partial t}\mu_\theta + \kappa \Delta\mu_\theta\big) h_\theta \, \mathrm{d}x \, \mathrm{d}t \\
& - \rho c \int_\Omega \mu_\theta(x, T) h_\theta(x, T) - \mu_\theta(x, 0) h_\theta(x, 0) \, \mathrm{d}x \\
& + \kappa \int_0^T \int_\Gamma \mu_\theta \tfrac{\partial}{\partial\nu} h_\theta \, \mathrm{d}x \, \mathrm{d}t - \kappa \int_0^T \int_\Gamma \tfrac{\partial}{\partial\nu}\mu_\theta h_\theta \, \mathrm{d}x \, \mathrm{d}t - \int_0^T \int_\Gamma \mu_\theta \tfrac{\partial}{\partial\nu} h_\theta \, \mathrm{d}x \, \mathrm{d}t.
\end{aligned}
$$

8

Then (16a)-(16c) is equivalent to

$$0 = \int_0^T \int_\Omega (\omega(\hat{\theta} - \theta^*) + \rho c \tfrac{\partial}{\partial t}\mu_\theta + \kappa \Delta \mu_\theta) h_\theta \; \mathrm{d}x \; \mathrm{d}t - \rho c \int_\Omega \mu_\theta(x, T) h_\theta(x, T) \; \mathrm{d}x$$

$$- \kappa \int_0^T \int_\Gamma \tfrac{\partial}{\partial \nu}\mu_\theta h_\theta \; \mathrm{d}x \; \mathrm{d}t$$

for all h_θ smooth enough with $h_\theta(x, 0) = 0$ on Ω and $\tfrac{\partial}{\partial \nu} h_\theta(x, t) = 0$ on $\Gamma \times \mathbb{I}$, which is satisfied if $\mu_\theta \in H^1(\Omega \times \mathbb{I})$ solves the adjoint equation

$$\begin{aligned}
-\rho c \tfrac{\partial}{\partial t}\mu_\theta - \kappa \Delta \mu_\theta &= \omega(\hat{\theta} - \theta^*) &&\text{on } \Omega \times \mathbb{I}, \\
\mu_\theta(x, T) &= 0 &&\text{on } \Omega, \\
\tfrac{\partial}{\partial \nu}\mu_\theta &= 0 &&\text{on } \Gamma \times \mathbb{I}.
\end{aligned}$$

Furthermore, using integration by parts we get

$$\begin{aligned}
\tfrac{\partial}{\partial s} L(s - \hat{s}) &= \beta \int_0^T \ddot{\hat{s}}(\ddot{s} - \ddot{\hat{s}}) \; \mathrm{d}t + \int_0^T \int_\Omega \mu_\theta \tfrac{\partial}{\partial l} F \tfrac{\partial}{\partial s} \gamma (s - \hat{s}) \; \mathrm{d}x \; \mathrm{d}t \\
&= \beta \ddot{\hat{s}}(\dot{s} - \dot{\hat{s}})|_0^T - \beta \hat{s}^{(3)}(s - \hat{s})|_0^T \\
&\quad + \int_0^T \left(\beta \hat{s}^{(4)} + \int_\Omega \mu_\theta \tfrac{\partial}{\partial l} F \tfrac{\partial}{\partial s} \gamma \; \mathrm{d}x \right)(s - \hat{s}) \; \mathrm{d}t.
\end{aligned}$$

Then it follows from (15) and (16d) that

$$\int_0^T \left(\beta \hat{s}^{(4)} + \int_\Omega \mu_\theta \tfrac{\partial}{\partial l} F \tfrac{\partial}{\partial s} \gamma \; \mathrm{d}x \right)(s - \hat{s}) \; \mathrm{d}t \geq 0 \quad \text{for all } s \in \mathcal{U}_{ad}^s.$$

The necessary condition (16e) for $\hat{u}_l$ takes the form

$$\tfrac{\partial}{\partial u_l} L(u_l - \hat{u}_l) = \int_0^T \left(\alpha \hat{u}_l + \int_\Omega \mu_\theta \tfrac{\partial}{\partial u_l} F \; \mathrm{d}x \right)(u_l - \hat{u}_l) \; \mathrm{d}t \geq 0 \quad \text{for all } u_l \in \mathcal{U}_{ad}^{u_l}.$$

Summarizing, we get the first-order optimality conditions

$$\rho c \tfrac{\partial}{\partial t}\hat{\theta} - \kappa \Delta \hat{\theta} = F \qquad\qquad \text{on} \quad \Omega \times \mathbb{I}, \qquad\qquad (17\text{a})$$
$$\hat{\theta}(x,0) = \theta_0 \qquad\qquad \text{on} \quad \Omega,$$
$$\tfrac{\partial}{\partial \nu}\hat{\theta}(x,t) = 0 \qquad\qquad \text{on} \quad \Gamma \times \mathbb{I},$$

$$-\rho c \tfrac{\partial}{\partial t}\mu_\theta - \kappa \Delta \mu_\theta = \omega(\hat{\theta} - \theta^*) \qquad\qquad \text{on} \quad \Omega \times \mathbb{I}, \qquad\qquad (17\text{b})$$
$$\mu_\theta(x,T) = 0 \qquad\qquad \text{on} \quad \Omega,$$
$$\tfrac{\partial}{\partial \nu}\mu_\theta(x,t) = 0 \qquad\qquad \text{on} \quad \Gamma \times \mathbb{I},$$

$$\int_0^T G_{u_l}(u_l - \hat{u}_l)\,\mathrm{d}t \geq 0 \qquad\qquad \text{for all} \quad u_l \in \mathcal{U}_{ad}^{u_l}, \qquad\qquad (17\text{c})$$

$$\int_0^T G_s(s - \hat{s})\,\mathrm{d}t \geq 0 \qquad\qquad \text{for all} \quad s \in \mathcal{U}_{ad}^{s}, \qquad\qquad (17\text{d})$$

where

$$G_{u_l} \;=\; \alpha u_l + \int_\Omega \mu_\theta \tfrac{\partial}{\partial u_l} F\,\mathrm{d}x, \qquad\qquad (17\text{e})$$

$$G_s \;=\; \beta s^{(4)} + \int_\Omega \mu_\theta \tfrac{\partial}{\partial l} F \tfrac{\partial}{\partial s}\gamma\,\mathrm{d}x. \qquad\qquad (17\text{f})$$

The used search directions $\tilde{G}_{u_l}$ and $\tilde{G}_s$ in the line search of the gradient based method are the scaled gradient functions, i.e., $\tilde{G}_{u_l} = \sigma_{u_l} G_{u_l}$ and $\tilde{G}_s = \sigma_s G_s$, where $\sigma_{u_l}, \sigma_s \in \mathbb{R}$ are chosen such that

$$\max_{t \in \mathbb{I}} |\tilde{G}_{u_l}| = 1 \quad \text{and} \quad \max_{t \in \mathbb{I}} |\tilde{G}_s| = 1.$$

In the odd and even gradient steps of the alternating line search, respectively, the laser position s and the laser power u_l are adjusted.

Example 3.1 (*Scenario I*) In this example, the initial controls are taken as $u_{l_{ini}}(t) \equiv 1000\,\text{W}$ and $s_{ini}(t) = t/(5\text{s})$ for $t \in \mathbb{I}$ such that the laser initially points directly into the center of the target region, i.e., $l(t) = \gamma(s_{ini}(t))$.
First, we aim to determine an optimal solution for the laser control u_l and the laser position s within the target curve $\gamma(\xi(t)) = \gamma_I(\xi(t))$ given in (13) without penalization of the laser acceleration. We set the regularization parameters to $\alpha = 10^{-5}$ and $\beta = 0$. The optimization results are illustrated in Figure 9. The optimization yields optimal controls, see Figures 9a) and 9b), which lead to a very good approximation $\hat{\theta}$ of the desired temperature $\theta^* = 1200\,\text{K}$ within the target region ω, see Figure 9d). Figure 9g) illustrates the laser treatment result. The dots along the laser acting
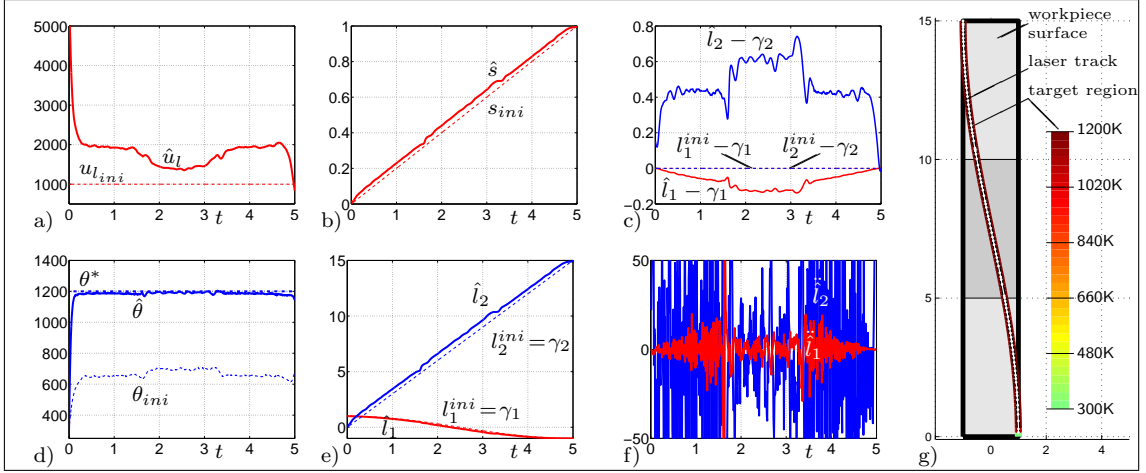
Figure 9: Laser position optimization for Scenario I with $\beta = 0$: a) initial and optimal laser controls $u_{l_{ini}}$ and $\hat{u}_l$, b) initial and optimal laser positions s_{ini} and $\hat{s}$ on the target curve γ, c) deviation of the laser acting point l from the center γ of the target region, d) initial, optimal, and desired temperature θ_{ini}, $\hat{\theta}$ and θ^* in the target region ω, e) initial and optimal laser track l_{ini} and $\hat{l}$, f) laser acceleration $\ddot{\hat{l}}$, g) laser treatment result on the target curve γ.

curve reflect the laser acting points at every fifth time step t_i of the numerical solution. This gives an idea of the speed of the laser along its track. Since the hottest point lies shortly behind the laser acting point depending on the laser velocity and the laser power, see [12], the laser acting point is guided in front of the center $\gamma(\xi(t))$ of the target region $\omega(t)$ moving along the target curve γ, i.e., $l_2(t) - \gamma_2(\xi(t)) > 0$, that justifies our choice for $\mathcal{U}^s_{ad}$. This behavior is illustrated in Figures 9c), e) and g). Caused by the highly reduced self-cooling of the workpiece above the hole, the laser is accelerated and the distance between the laser acting point $l(t)$ and the center of the target region on $\gamma(\xi(t))$ is increased shortly behind the beginning of the hole. On the other hand, shortly behind the hole, the laser is slowed down such that the gap between $l(t)$ and $\gamma(\xi(t))$ decreases since the self-cooling of the workpiece comes into play again. This behavior is in agreement with the results in [12].

Because of the unrealizable large laser accelerations, see Figure 9f), in the following we will use $\beta = 10$ to penalize large accelerations of the laser acting point. The regularization parameter α remains unchanged $\alpha = 10^{-5}$. The optimization results are illustrated in Figure 10. As we can see, the acceleration of the laser acting point is strongly reduced such that this solution is more suitable for industrial robots guiding the laser, compare Figures 9f) and 10f). However, it should be noted that the small accelerations of the laser acting point are compensated with a more oscillating and slightly higher laser power, compare Figures 9a) and 10a). Nevertheless, the production goal is satisfied very well, see Figure 10d). ◁
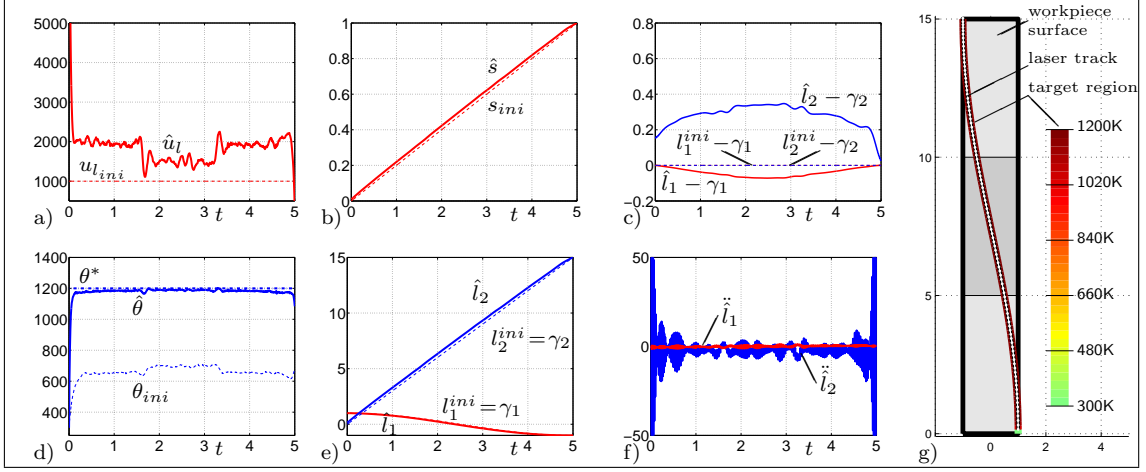
Figure 10: Laser position optimization for Scenario I with $\beta = 10$: a) initial and optimal laser controls $u_{l_{ini}}$ and $\hat{u}_l$, b) initial and optimal laser positions s_{ini} and $\hat{s}$ on the target curve γ, c) deviation of the laser acting point l from the center γ of the target region, d) initial, optimal, and desired temperature θ_{ini}, $\hat{\theta}$ and θ^* in the target region ω, e) initial and optimal laser track l_{ini} and $\hat{l}$, f) laser acceleration $\ddot{\hat{l}}$, g) laser treatment result on the target curve γ.

Example 3.2 (*Scenario II*) As in Example 3.1, again the production goal is to reach the desired temperature profile $\theta^* = 1200\,\text{K}$ within the target region ω, but now, moving along the target curve $\gamma = \gamma_{I\!I}$ given in (13). The initial controls are given again as $u_{l_{ini}}(t) \equiv 1000\,\text{W}$ and $s_{ini}(t) = t/(5\text{s})$ for $t \in \mathbb{I}$ such that the laser initially points into the center of the moving target region, i.e., $l(t) = \gamma(s_{ini}(t))$. We use first the regularization parameters $\alpha = 10^{-5}$ and $\beta = 0$.

The numerical results of the optimization are presented in Figure 11. The obtained temperature $\hat{\theta}$ in the target region matches the desired one very well, see Figure 11d). Therefore, the production goal is achieved. However, the use of $\beta = 0$ again results in large oscillating acceleration $\ddot{s}$ of the laser acting point within the target curve γ because large values of $\ddot{s}$ are not penalized in the objective functional. This leads to extremely large accelerations $\ddot{l}$ of the laser acting point as illustrated in Figure 11f). In general, this laser path is not realizable for industrial robots.

To reduce the oscillations in $\ddot{s}$ and to improve the realizability, we increase again the parameter β to $\beta = 0.01$, while α remains unchanged. The obtained numerical results are presented in Figure 12. The production goal is satisfied very well, see Figure 12d). Although the high acceleration of the laser is reduced as long as the target curve is smooth, the acceleration of the laser passing the corners in the target curve is still infinitely large, see Figure 12f), and therefore, again not realizable by use of industrial robots guiding the robot. Nevertheless, the interaction between the laser track and the laser power is as expected, see Figure 12c).   ◁

The examples above suggest that this approach for the laser power and laser position optimization is suitable as long as the curvature of the target curve γ remains in
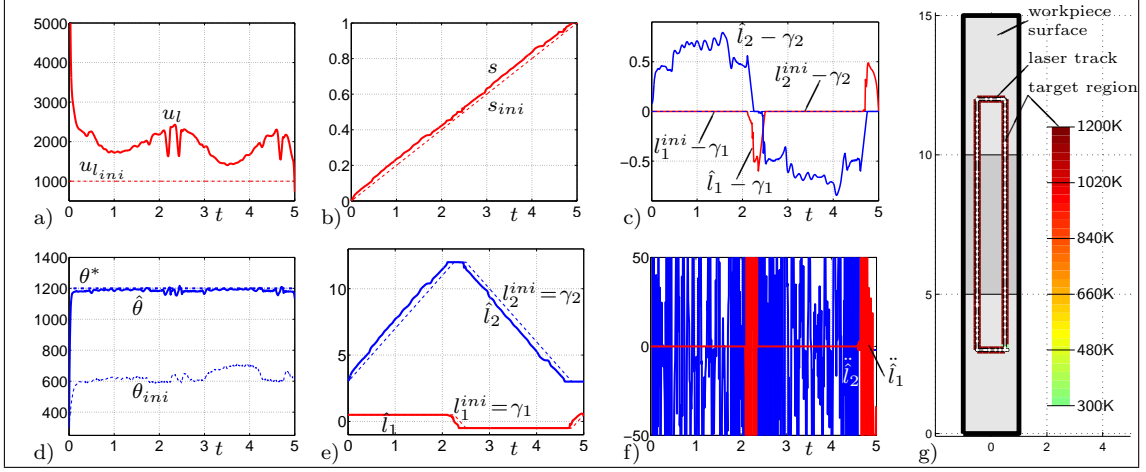
Figure 11: Laser position optimization for Scenario II with $\beta = 0$: a) initial and optimal laser controls $u_{l_{ini}}$ and $\hat{u}_l$, b) initial and optimal laser positions s_{ini} and $\hat{s}$ on the target curve γ, c) deviation of the laser acting point l from the center γ of the target region, d) initial, optimal, and desired temperature θ_{ini}, $\hat{\theta}$ and θ^* in the target region ω, e) initial and optimal laser track l_{ini} and $\hat{l}$, f) laser acceleration $\ddot{\hat{l}}$, g) laser treatment result on the target curve γ.
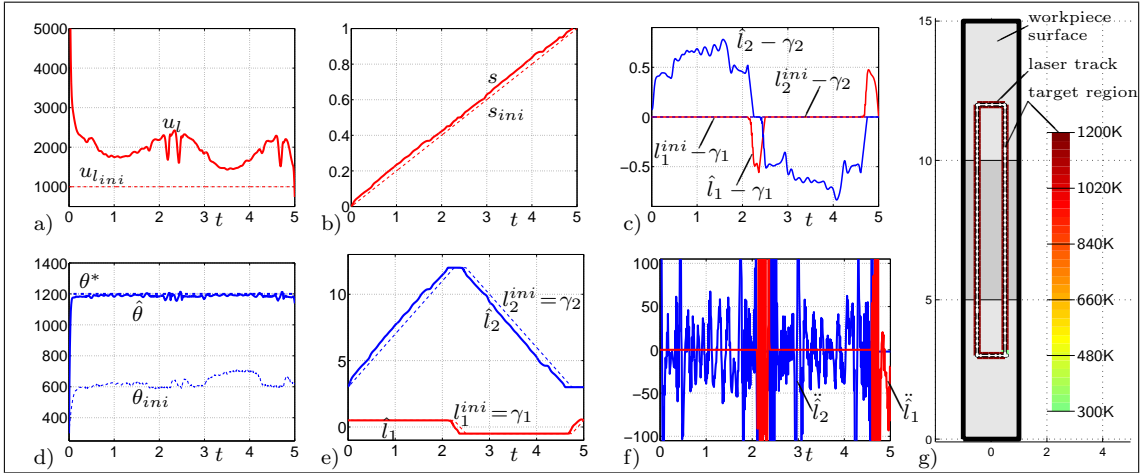

Figure 12: Laser position optimization for Scenario II with $\beta = 0.01$: a) initial and optimal laser controls $u_{l_{ini}}$ and $\hat{u}_l$, b) initial and optimal laser positions s_{ini} and $\hat{s}$ on the target curve γ, c) deviation of the laser acting point l from the center γ of the target region, d) initial, optimal, and desired temperature θ_{ini}, $\hat{\theta}$ and θ^* in the target region ω, e) initial and optimal laser track l_{ini} and $\hat{l}$, f) laser acceleration $\ddot{\hat{l}}$, g) laser treatment result in the target curve γ.

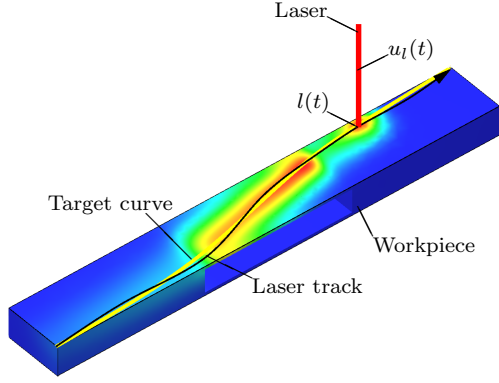certain bounds depending on the acceleration bounds of the robot.

13

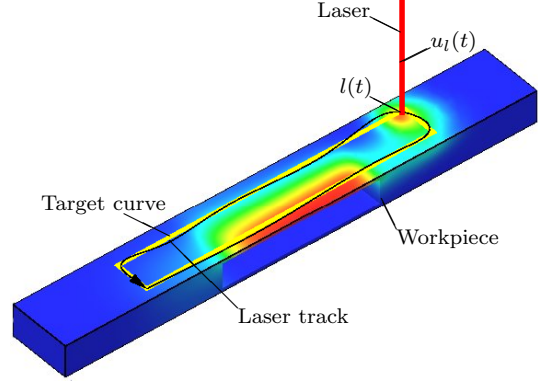Figure 13: Laser track optimization of Scenario I

Figure 14: Laser track optimization of Scenario II

3.3 Laser Power and Laser Track Optimization

In this approach, we will use the *laser track l* on the workpiece surface Γ itself as optimization variables. Since we restrict our considerations to workpieces with machined surface Γ lying in the $\{z = 0\}$ plane, the laser track is defined as $l = [l_1, l_2, 0]^T$. In the following we will drop the third coordinate and use $l = [l_1, l_2]^T$ as a control in addition to the laser power u_l.

Therefore, we want to determine optimal functions $u_l \in \mathcal{U}_{ad}^{u_l}$ and $l \in \mathcal{U}_{ad}^l$ minimizing the cost functional

$$J(u_l, l) = J_\theta + J_R = J_\theta + \frac{\alpha}{2} \int_0^T u_l(t)^2 \, \mathrm{d}t + \frac{\beta}{2} \int_0^T ||\ddot{l}(t)||_2^2 \, \mathrm{d}t$$

subject to the heat equation (5). Here, the admissible set $\mathcal{U}_{ad}^l$ is given by

$$\mathcal{U}_{ad}^l = \{\, l \in C^4(\mathbb{I}, \mathbb{R}^2) \;\; | \;\; \ddot{l}(0) = \ddot{l}(T) = 0, \;\; l^{(3)}(0) = l^{(3)}(T) = 0 \,\}. \tag{18}$$

With the Lagrange multipliers μ_θ the Lagrange function is given by

$$
\begin{aligned}
L(\theta, l, u_l, \mu_\theta) \;=\;\; & \frac{1}{2} \int_0^T \int_\Omega \omega(\theta - \theta^*)^2 \, \mathrm{d}x \, \mathrm{d}t + \frac{\alpha}{2} \int_0^T u_l^2 \, \mathrm{d}t + \frac{\beta}{2} \int_0^T ||\ddot{l}||_2^2 \, \mathrm{d}t \\
& - \int_0^T \int_\Omega \mu_\theta (\rho c \tfrac{\partial}{\partial t}\theta - \kappa \Delta \theta - F) \, \mathrm{d}x \, \mathrm{d}t - \int_0^T \int_\Gamma \mu_\theta \tfrac{\partial}{\partial \nu}\theta \, \mathrm{d}x \, \mathrm{d}t.
\end{aligned}
$$

Necessary conditions for a stationary point $(\hat{\theta}, \hat{l}, \hat{u}_l)$ to be optimal is that the relations

$$\frac{\partial}{\partial \theta} L h_\theta = 0 \qquad \text{on} \quad \Omega \times \mathbb{I}, \tag{19a}$$

$$h_\theta(x, 0) = 0 \qquad \text{on} \quad \Omega, \tag{19b}$$

$$\frac{\partial}{\partial \nu} h_\theta(x, t) = 0 \qquad \text{on} \quad \Gamma \times \mathbb{I}, \tag{19c}$$

$$\frac{\partial}{\partial l} L(l - \hat{l}) \geq 0, \tag{19d}$$

$$\frac{\partial}{\partial u_l} L(u_l - \hat{u}_l) \geq 0 \tag{19e}$$

are satisfied for all suitable test functions h_θ, as well as $l \in \mathcal{U}_{ad}^l$ and $u_l \in \mathcal{U}_{ad}^{u_l}$. The conditions (19a) and (19e) are the same as in the previous approach (Section 3.2) and, therefore, they correspond to (17b) and (17c) with (17e).

Using integration by parts, we obtain from (19d) that

$$
\begin{aligned}
\frac{\partial}{\partial l} L(l - \hat{l}) &= \beta \int_0^T \ddot{\hat{l}}^T (\ddot{l} - \ddot{\hat{l}}) \, \mathrm{d}t + \int_0^T \int_\Omega \mu_\theta \frac{\partial}{\partial l} F(l - \hat{l}) \, \mathrm{d}x \, \mathrm{d}t \\
&= \beta \ddot{\hat{l}}^T (\dot{l} - \dot{\hat{l}})|_0^T - \beta (\hat{l}^{(3)})^T (l - \hat{l})|_0^T \\
&\quad + \int_0^T \left(\beta (\hat{l}^{(4)})^T + \int_\Omega \mu_\theta \frac{\partial}{\partial l} F \, \mathrm{d}x \right) (l - \hat{l}) \, \mathrm{d}t.
\end{aligned}
$$

Taking into account (18) and (19d), we get the condition

$$\int_0^T \left(\beta (\hat{l}^{(4)})^T + \int_\Omega \mu_\theta \frac{\partial}{\partial l} F \, \mathrm{d}x \right) (l - \hat{l}) \, \mathrm{d}t \geq 0 \quad \text{for all} \ \ l \in \mathcal{U}_{ad}^l.$$

Summarizing, we obtain the first-order optimality conditions

$$\rho c \frac{\partial}{\partial t} \hat{\theta} - \kappa \Delta \hat{\theta} = F \qquad \text{on} \quad \Omega \times \mathbb{I}, \tag{20a}$$
$$\hat{\theta}(x, 0) = \theta_0 \qquad \text{on} \quad \Omega,$$
$$\frac{\partial}{\partial \nu} \hat{\theta}(x, t) = 0 \qquad \text{on} \quad \Gamma \times \mathbb{I},$$

$$-\rho c \frac{\partial}{\partial t} \mu_\theta - \kappa \Delta \mu_\theta = \omega(\hat{\theta} - \theta^*) \qquad \text{on} \quad \Omega \times \mathbb{I}, \tag{20b}$$
$$\mu_\theta(x, T) = 0 \qquad \text{on} \quad \Omega,$$
$$\frac{\partial}{\partial \nu} \mu_\theta(x, t) = 0 \qquad \text{on} \quad \Gamma \times \mathbb{I},$$

$$\int_0^T G_{u_l}(u_l - \hat{u}_l) \, \mathrm{d}t \geq 0 \qquad \text{for all} \quad u_l \in \mathcal{U}_{ad}^{u_l}, \tag{20c}$$

$$\int_0^T G_l(l - \hat{l}) \, \mathrm{d}t \geq 0 \qquad \text{for all} \quad l \in \mathcal{U}_{ad}^l, \tag{20d}$$

15

where

$$G_{u_l} = \alpha u_l + \int_\Omega \mu_\theta \frac{\partial}{\partial u_l} F \; dx, \tag{20e}$$

$$G_l = \beta (l^{(4)})^T + \int_\Omega \mu_\theta \frac{\partial}{\partial l} F \; dx. \tag{20f}$$

The used search directions $\tilde{G}_{u_l}$ and $\tilde{G}_l$ in the line search of the gradient based method are the scaled gradient functions, i.e., $\tilde{G}_{u_l} = \sigma_{u_l} G_{u_l}$ and $\tilde{G}_l = \sigma_l G_l$, where $\sigma_{u_l}, \sigma_l \in \mathbb{R}$ are chosen such that

$$\max_{t \in \mathbb{I}} |\tilde{G}_{u_l}| = 1 \quad \text{and} \quad \max_{t \in \mathbb{I}} |\tilde{G}_l| = 1.$$

In odd gradient steps of the alternating line search the laser position l will be adjusted and in even ones the laser power u_l.

Example 3.3 (*Scenario I*) In comparison to Example 3.1, the control variables for the laser are changed such that the laser track l is now used as an optimization variable instead of the laser position s. The initial controls are taken as $u_{l_{ini}}(t) \equiv 1000\,\text{W}$ and $l_{ini}(t) = \gamma_I(t/(5\text{s}))$ for $t \in \mathbb{I}$ such that the laser initially points into the center of the target region.
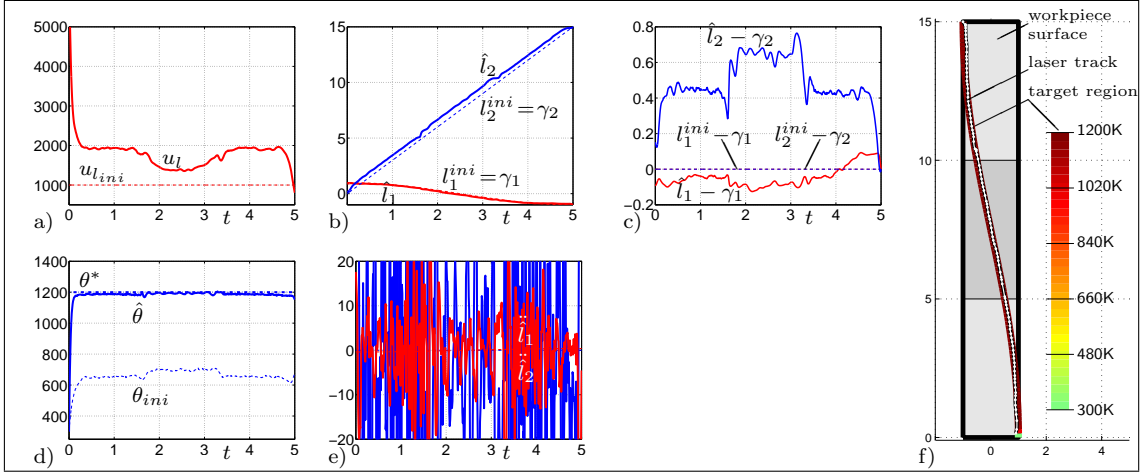

Figure 15: Laser track optimization for Scenario I with $\beta = 0$: a) initial and optimal laser controls $u_{l_{ini}}$ and $\hat{u}_l$, b) initial and optimal laser track l_{ini} and $\hat{l}$ on the work piece surface, c) deviation of the laser acting point l from the center γ of the target region, d) initial, optimal, and desired temperature θ_{ini}, $\hat{\theta}$ and θ^* in the target region ω, e) laser acceleration $\ddot{\hat{l}}$, f) laser treatment result in the target curve γ.

In Figure 15, we present the numerical results for the regularization parameters $\alpha = 10^{-5}$ and $\beta = 0$. Since in this approach the laser track l on the surface Γ is used as a control variable, the laser acting curve l is not restricted to the target curve γ. In particular, in the starting and final points, the obtained laser acting

16

curve l differs from the target curve $\gamma = \gamma_I$. Figure 15d) shows that the obtained temperature $\hat{\theta}$ in the target region satisfies the production goal very well. Again as in Example 3.1, the control of the laser track reacts on the missing self-cooling effect above the hole in the workpiece such that the distance between the target region and the laser acting point increases, see Figures 15b) and 15c).

Unfortunately, the absence of the penalization of accelerations of the laser acting point leads to large accelerations as shown in Figure 15e) and, therefore, to a laser track which is not realizable by industrial robots. Increasing the penalty parameter to $\beta = 10$, we obtain the optimization results shown in Figure 16. In contrast to the numerical results obtained for $\beta = 0$, the acceleration of the laser acting point is now strongly reduced, compare Figures 15e) and 16e), and can be realized by industrial robots. Furthermore, the distance between the target region and the laser acting point behaves in a more moderate way, see Figures 16b) and c), and is compensated by a more varying and slightly increased laser power, see Figure 16a). Concluding, the production goal is now achieved in a more practicable way, see Figure 16f). ◁
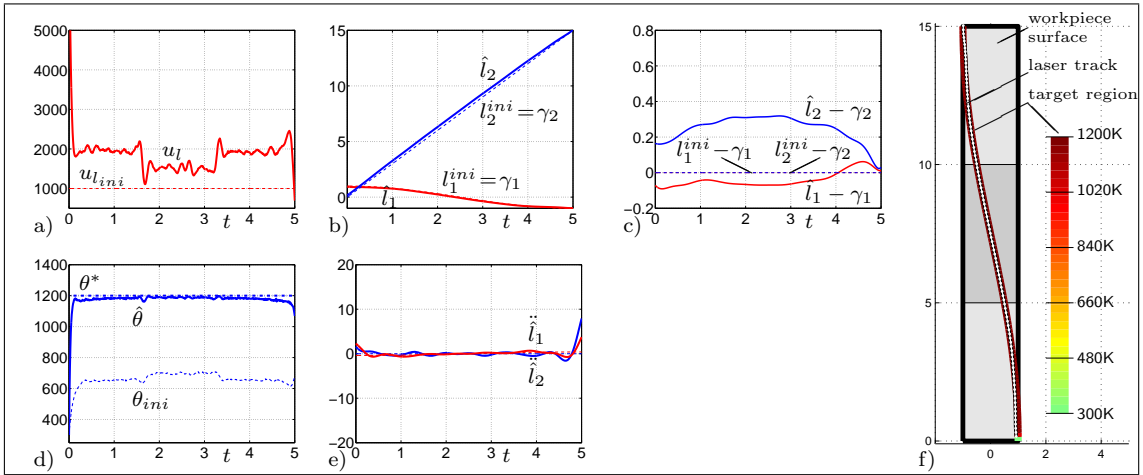

Figure 16: Laser track optimization for Scenario I with $\beta = 10$: a) initial and optimal laser controls $u_{l_{ini}}$ and $\hat{u}_l$, b) initial and optimal laser track l_{ini} and $\hat{l}$ on the work piece surface, c) deviation of the laser acting point l from the center γ of the target region, d) initial, optimal, and desired temperature θ_{ini}, $\hat{\theta}$ and θ^* in the target region ω, e) laser acceleration $\ddot{l}$, f) laser treatment result on the target curve γ.

Example 3.4 (*Scenario $\mathbb{II}$*) Let us now consider again Scenario $\mathbb{II}$, where, in contrast to Example 3.2, the laser track l is used as control variable.

The initial controls are given as $u_{l_{ini}}(t) \equiv 1000\,\text{W}$ and $l_{ini}(t) = \gamma_{\mathbb{II}}(t/(5\text{s}))$ for $t \in \mathbb{I}$ such that the laser initially points into the center of the target region. We use first the regularization parameters $\alpha = 10^{-5}$ and $\beta = 0$. The optimization results are depicted in Figure 17. As shown in Figure 17d), the production goal is satisfied very well. Figures 17b) and 17c) show the displacement of the laser acting curve
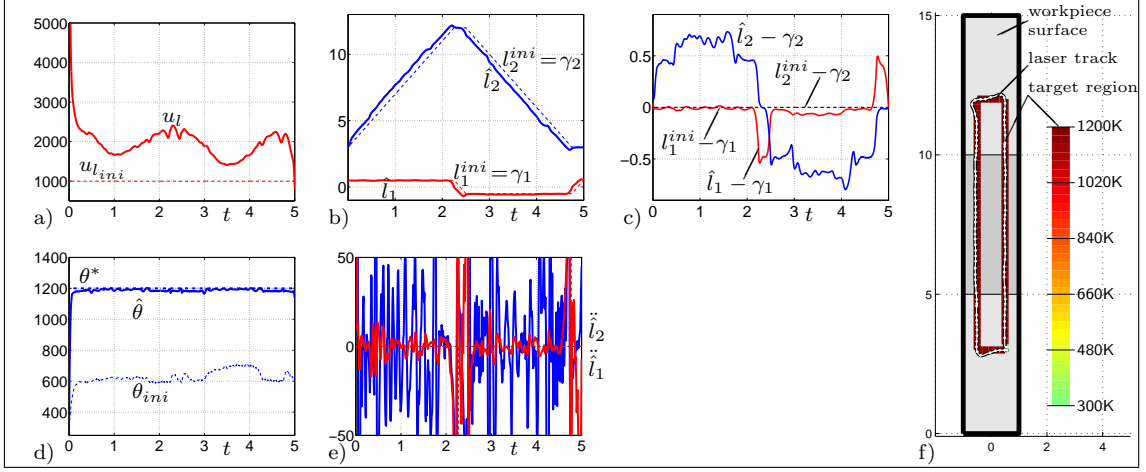
Figure 17: Laser track optimization for Scenario $\mathbb{II}$ with $\beta = 0$: a) initial and optimal laser controls $u_{l_{ini}}$ and $\hat{u}_l$, b) initial and optimal laser track l_{ini} and $\hat{l}$ on the work piece surface, c) deviation of the laser acting point l from the center γ of the target region, d) initial, optimal, and desired temperature θ_{ini}, $\hat{\theta}$ and θ^* in the target region ω, e) laser acceleration $\ddot{\hat{l}}$, f) laser treatment result on the target curve γ.
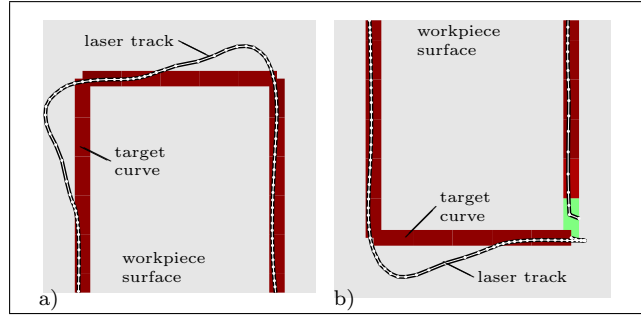

Figure 18: Laser track optimization for Scenario $\mathbb{II}$ with $\beta = 0$: laser treatment result (zoom).

l in front of the target region γ (which corresponds to l_{ini}) and also the increasing distance above the hole in the workpiece. However, due to the missing penalization ($\beta = 0$) we obtain again large acceleration of the laser acting point, see Figure 17e), and a rather laser track, see Figure 18. This is difficult to be realized by industrial robots. Note that in Figure 18 the dots along the laser acting curve represent the laser acting points at the time steps t_i. Here, one can see that the speed of the laser acting point varies strongly along the laser acting curve because of large accelerations, see Figure 17e). Nevertheless, these large accelerations can be reduced by increasing the penalty parameter to $\beta = 0.01$. The regularization parameter α remains unchanged. The numerical optimization results in this case are shown in Figure 19. The obtained temperature $\hat{\theta}$ in the target region fits almost the desired one θ^*, see Figure 19d), such that the production goal is achieved. Furthermore, the acceleration of the laser is smoother and smaller than in Example 3.2, compare
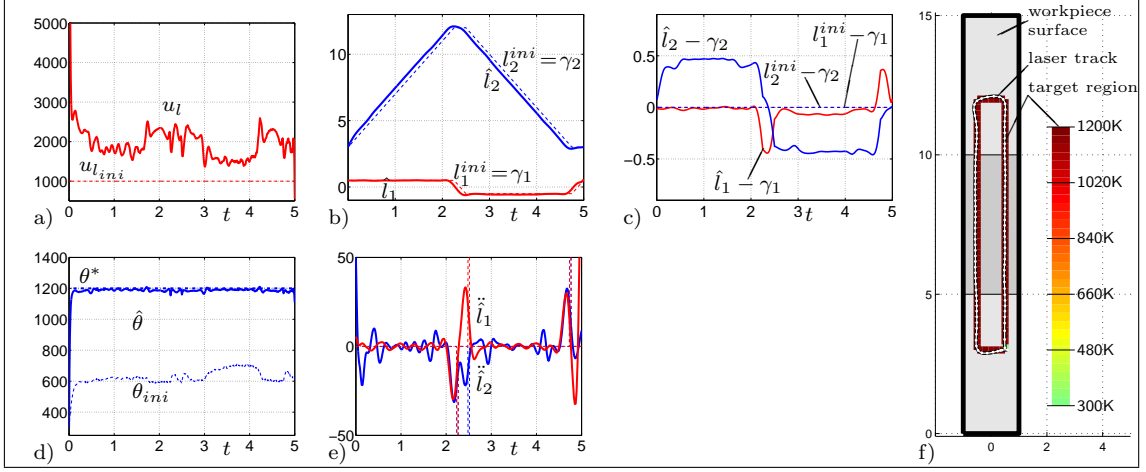
Figure 19: Laser track optimization of Scenario $\mathbb{II}$ with $\beta = 0.01$: a) initial and optimal laser controls $u_{l_{ini}}$ and $\hat{u}_l$, b) initial and optimal laser track l_{ini} and $\hat{l}$ on the work piece surface, c) deviation of the laser acting point l from the center γ of the target region, d) initial, optimal, and desired temperature θ_{ini}, $\hat{\theta}$ and θ^* in the target region ω, e) laser acceleration $\ddot{\hat{l}}$, f) laser treatment result in the target curve γ,
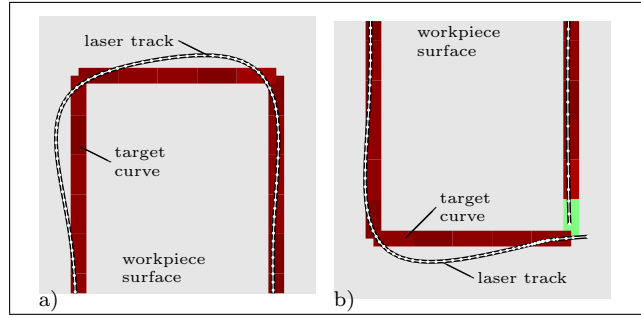

Figure 20: Laser track optimization of Scenario $\mathbb{II}$ with $\beta = 0.01$: laser treatment result (zoom)

Figure 12f) and Figure 19e). Note that we have also a smoother laser track, see Figure 20 in comparison to Figure 18. ◁

Thus, we may conclude that this approach for the laser power and laser track optimization is realizable by industrial robots even in the case of nonsmooth target curves as long as the penalization of the acceleration of the laser track is used.

3.4 Laser Power and Robot Control Optimization

In this approach, we consider the optimal control of robot guided laser treatment. Our goal is to determine an optimal laser power $u_l \in \mathcal{U}_{ad}^{u_l}$ and an optimal robot
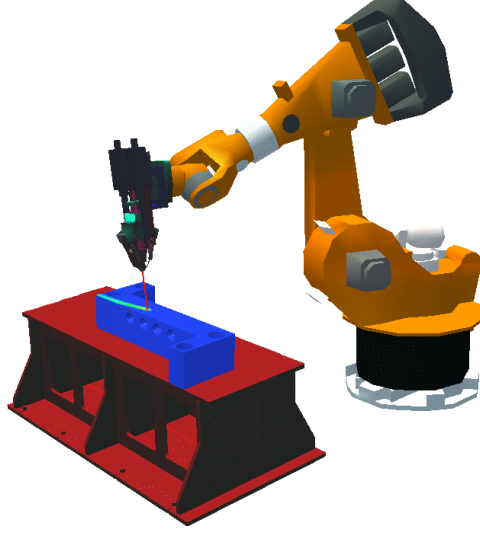
Figure 21: Laser power and robot motion/control optimization

control $u_r \in \mathcal{U}_{ad}^{u_r}$ that minimize the cost functional

$$J(u_l, u_r) = J_\theta + J_R = J_\theta + \frac{\alpha}{2} \int\limits_0^T u_l(t)^2 \, \mathrm{d}t + \frac{\beta}{2} \int\limits_0^T ||u_r(t)||_2^2 \, \mathrm{d}t$$

subject to the heat equation (5) coupled with the equations of motion (11) for the robot. The laser track is now given as a function of q, i.e, $l = l(q)$.

With the Lagrange multipliers $\mu = [\,\mu_q^T, \ \mu_\theta\,]^T$, the Lagrange function is given by

$$
\begin{aligned}
L(\theta, q, u_r, u_l, \mu) \;=\; & \frac{1}{2} \int\limits_0^T \int\limits_\Omega \omega(\theta - \theta^*)^2 \, \mathrm{d}x \, \mathrm{d}t + \frac{\alpha}{2} \int\limits_0^T u_l^2 \, \mathrm{d}t + \frac{\beta}{2} \int\limits_0^T ||u_r||_2^2 \, \mathrm{d}t \\
& - \int\limits_0^T \mu_q^T (\dot{q} - k) \, \mathrm{d}t - \int\limits_0^T \int\limits_\Omega \mu_\theta (\rho c \tfrac{\partial}{\partial t}\theta - \kappa \Delta \theta - F) \, \mathrm{d}x \, \mathrm{d}t \\
& - \int\limits_0^T \int\limits_\Gamma k\mu_\theta \tfrac{\partial}{\partial \nu}\theta \, \mathrm{d}x \, \mathrm{d}t
\end{aligned}
$$

20

Necessary conditions for a stationary point $(\hat{\theta}, \hat{q}, \hat{u}_r, \hat{u}_l)$ is that the relations

$$\tfrac{\partial}{\partial \theta} L h_\theta = 0 \qquad \text{on} \quad \Omega \times \mathbb{I}, \tag{21a}$$

$$h_\theta(x, 0) = 0 \qquad \text{on} \quad \Omega, \tag{21b}$$

$$\tfrac{\partial}{\partial \nu} h_\theta(x, t) = 0 \qquad \text{on} \quad \Gamma \times \mathbb{I}, \tag{21c}$$

$$\tfrac{\partial}{\partial q} L h_q = 0 \qquad \text{on} \quad \mathbb{I}, \tag{21d}$$

$$h_q(0) = 0, \tag{21e}$$

$$\tfrac{\partial}{\partial u_r} L(u_r - \hat{u}_r) \geq 0, \tag{21f}$$

$$\tfrac{\partial}{\partial u_l} L(u_l - \hat{u}_l) \geq 0 \tag{21g}$$

are satisfied for all suitable test functions h_θ and h_q, as well as for $u_r \in \mathcal{U}_{ad}^{u_r}$ and $u_l \in \mathcal{U}_{ad}^{u_l}$. The conditions (21a)-(21c) and (21g) are the same as in Section 3.2 and, therefore, they correspond to (17b) and (17c) with (17e).

Using integration by parts we have

$$\tfrac{\partial}{\partial q} L h_q = -\int_0^T \mu_q^T \dot{h}_q \, dt + \int_0^T \mu_q^T \tfrac{\partial}{\partial q} k h_q \, dt + \int_0^T \int_\Omega \mu_\theta \tfrac{\partial}{\partial l} F \tfrac{\partial}{\partial q} l h_q \, dx \, dt$$

$$= \int_0^T \left(\int_\Omega \mu_\theta \tfrac{\partial}{\partial l} F \tfrac{\partial}{\partial q} l \, dx + \dot{\mu}_q^T + \mu_q^T \tfrac{\partial}{\partial q} k h_q \right) h_q \, dt - \mu_q^T h_q |_0^T.$$

Then (21d,)21e) is equivalent to

$$0 = \int_0^T \left(\int_\Omega \mu_\theta \tfrac{\partial}{\partial l} F \tfrac{\partial}{\partial q} l \, dx + \dot{\mu}_q^T + \mu_q^T \tfrac{\partial}{\partial q} k h_q \right) h_q \, dt - \mu_q^T(T) h_q(T)$$

for all h_q with $h_q(0) = 0$, which is satisfied if μ_q solves the adjoint equation

$$\dot{\mu}_q^T = -\int_\Omega \mu_\theta \tfrac{\partial}{\partial l} F \tfrac{\partial}{\partial q} l \, dx - \mu_q^T \tfrac{\partial}{\partial q} k \qquad \text{on} \quad \mathbb{I},$$

$$\mu_q(T) = 0.$$

Furthermore, the necessary condition (21d) for u_r takes the form

$$\tfrac{\partial}{\partial u_r} L(u_r - \hat{u}_r) = \int_0^T \left(\beta \hat{u}_r^T + \mu_q^T \tfrac{\partial}{\partial u_r} k \right)(u_r - \hat{u}_r) \, dt \geq 0 \quad \text{for all} \quad u_r \in \mathcal{U}_{ad}^{u_r}.$$

Summarizing, the first-order optimality conditions are stated as

$$\rho c \frac{\partial}{\partial t}\hat{\theta} - \kappa \Delta \hat{\theta} = F \qquad \text{on} \quad \Omega \times \mathbb{I}, \tag{22a}$$
$$\hat{\theta}(x,0) = \theta_0 \qquad \text{on} \quad \Omega,$$
$$\frac{\partial}{\partial \nu}\theta(x,t) = 0 \qquad \text{on} \quad \Gamma \times \mathbb{I},$$

$$\dot{\hat{q}} = k(\hat{q}, \hat{u}_r, t) \qquad \text{on} \quad \mathbb{I} \tag{22b}$$
$$\hat{q}(0) = q_0,$$

$$-\rho c \frac{\partial}{\partial t}\mu_\theta - \kappa \Delta \mu_\theta = \omega(\hat{\theta} - \theta^*) \qquad \text{on} \quad \Omega \times \mathbb{I}, \tag{22c}$$
$$\mu_\theta(x,T) = 0 \qquad \text{on} \quad \Omega,$$
$$\frac{\partial}{\partial \nu}\mu_\theta(x,t) = 0 \qquad \text{on} \quad \Gamma \times \mathbb{I},$$

$$\dot{\mu}_q^T = -\int_\Omega \mu_\theta \frac{\partial}{\partial q}F \, \mathrm{d}x - \mu_q^T \frac{\partial}{\partial q}k(\hat{q}, \hat{u}_r, t) \qquad \text{on} \quad \mathbb{I}, \tag{22d}$$
$$\mu_q^T(T) = 0,$$

$$\int_0^T G_{u_l}(u_l - \hat{u}_l) \, \mathrm{d}t \geq 0 \qquad \text{for all} \quad u_l \in \mathcal{U}_{ad}^{u_l}, \tag{22e}$$

$$\int_0^T G_{u_r}(u_r - \hat{u}_r) \, \mathrm{d}t \geq 0 \qquad \text{for all} \quad u_r \in \mathcal{U}_{ad}^{u_r}, \tag{22f}$$

where

$$G_{u_l} = \alpha u_l + \int_\Omega \mu_\theta \frac{\partial}{\partial u_l}F \, \mathrm{d}x,$$
$$G_{u_r} = \beta u_r^T + \mu_q^T \frac{\partial}{\partial u_r}k.$$

Note that the initial point $l(0)$ of the laser track is now determined by the initial state $q(0)$ of the robot.

The used search directions $\tilde{G}_{u_l}$ and $\tilde{G}_{u_r}$ in the line search of the gradient based method are the scaled gradient functions, i.e., $\tilde{G}_{u_l} = \sigma_{u_l}G_{u_l}$ and $\tilde{G}_{u_r} = \sigma_{u_r}G_{u_r}$, where $\sigma_{u_l}, \sigma_{u_r} \in \mathbb{R}$ are chosen such that

$$\max_{t \in \mathbb{I}} |\tilde{G}_{u_l}| = 10 \quad \text{and} \quad \max_{t \in \mathbb{I}} ||\tilde{G}_{u_r}||_\infty = 0.1.$$

In odd gradient steps of the alternating line search, the robot control u_r is improved, while in even ones the laser power u_l is improved.

Example 3.5 (*Scenario I*) In this example, the production goal is the same as in Examples 3.1 and 3.3. In our experiments, we use data for the KUKA robot KR 150

shown in Figure 21 to guide the laser. This is a robot with 6 axis. We use, however, only the first three axis as control variables u_r and force the remaining axis to keep the laser perpendicular to the workpiece surface.

The initially given laser control is $u_{l_{ini}}(t) \equiv 1000\,\text{W}$, for $t \in \mathbb{I}$, while the control variables of the robot respecting the motion of the laser acting point are initially chosen such that the laser initially follows the center of the moving target region, i.e., $l(t) = \gamma_I(t/(5\text{s}))$. In particular, the initial robot control $u_{r_{ini}}(t)$ is computed using the equations of motion (11) with prescribed $q(t)$ and $\dot{q}(t)$ obtained by inverse kinematic approach performed by INVISION.
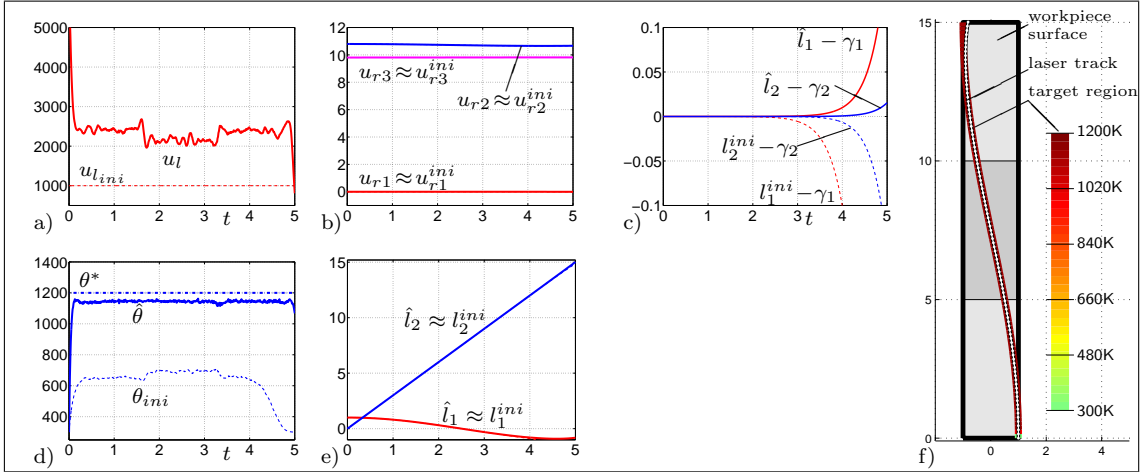

Figure 22: Robot control optimization of Scenario I with $\beta = 0$: a) initial and optimal laser controls $u_{l_{ini}}$ and $\hat{u}_l$, b) initial and optimal robot controls $u_{r_{ini}}$ and $\hat{u}_r$,, c) deviation of the laser acting point l from the center γ of the target region, d) initial, optimal, and desired temperature θ_{ini}, $\hat{\theta}$ and θ^* in the target region ω, e) initial and optimal laser track l_{ini} and $\hat{l}$, f) laser treatment result in the target curve γ

For the regularization parameters $\alpha = 10^{-5}$ and $\beta = 0$, we get the following optimization results shown in Figure 22. In contrast to Examples 3.1 and 3.3, the laser acting curve remains almost unchanged and, as a consequence, the laser points still into the center of the target region, see Figures 22c) and e). Therefore, the laser power has to be much larger than in the other both approaches, see Figure 22a) in comparison to, e.g., Figures 10a) or 16a). Unfortunately, the obtained temperature $\hat{\theta}$ in the target region does not reach the desired $\theta^* = 1200\,\text{K}$ due to the costs caused from the higher laser power. Consequently, the obtained result of the optimization does not satisfy the production goal. ◁

Example 3.6 (*Scenario II*) As last example let us now consider again Scenario II, where the heat equation (5) is coupled with the equations of motion (11) for the robot KR 150.

Again, the initially given laser control is $u_{l_{ini}}(t) \equiv 1000\,\text{W}$, for $t \in \mathbb{I}$, while the control variables of the robot respecting the motion of the laser acting point are

initially chosen such that the laser initially follows the center of the moving target region, i.e., $l(t) = \gamma_{\mathbb{II}}(t/(5s))$. In particular, the initial robot control $u_{r_{ini}}(t)$, is computed using the equations of motions (11) with prescribed $q(t)$ and $\dot{q}(t)$ provided by INVISION.
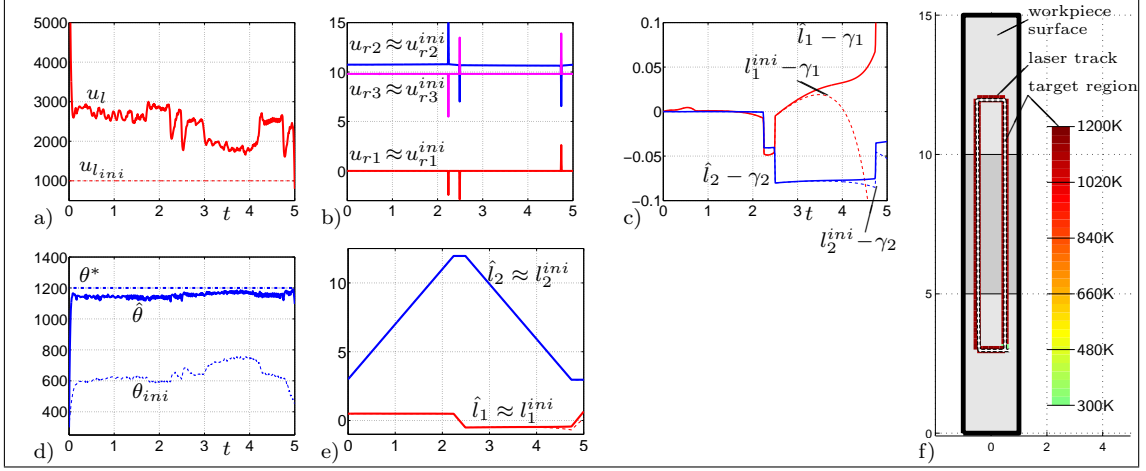

Figure 23: Robot control optimization for Scenario $\mathbb{II}$ with $\beta = 0$: a) initial and optimal laser controls $u_{l_{ini}}$ and $\hat{u}_l$, b) initial and optimal robot controls $u_{r_{ini}}$ and $\hat{u}_r$,, c) deviation of the laser acting point l from the center γ of the target region, d) initial, optimal, and desired temperature θ_{ini}, $\hat{\theta}$ and θ^* in the target region ω, e) initial and optimal laser track l_{ini} and $\hat{l}$, f) laser treatment result on the target curve γ.

The numerical results obtained for $\alpha = 10^{-5}$ and $\beta = 0$ are presented in Figure 23. Again, the laser acting curve is almost unchanged such that the laser points still into the center of the target region except in the end of the laser track, see Figure 23c). Due to the higher speed of the laser acting point in this example in contrast to Example 3.5, the laser power has to be even larger, compare Figure 23a) with, e.g., Figures 12a) or 19a). Furthermore, Figure 23d) shows that the desired temperature θ^* is almost reached in the second half of the time interval $\mathbb{II}$ only. Thus, the obtained result of the optimization does not satisfy the production goal very well. ◁

Both examples above show representative for many other examples that the approach presented in this section, i.e., the laser power and robot control optimization, in general, is not suitable. Unfortunately, gradient based methods reacts too sensitive to changes in the robot control. In particular, small changes in the robot control at the beginning of the interval $\mathbb{II}$ have a great influence on the laser track at the end of $\mathbb{II}$. Therefore, the gradient method has to perform very small gradient steps to improve the objective functional over the whole interval $\mathbb{II}$ leading to an extremely slow convergence such that the optimization have to be stopped unsuccessfully.

4 Summary

In this paper, we introduced and discussed several approaches for the optimal control of robot guided laser material treatments.
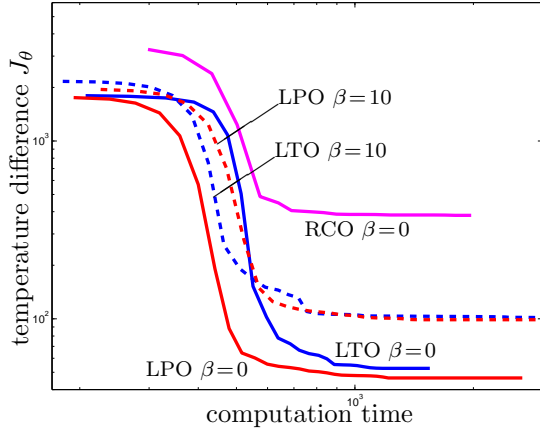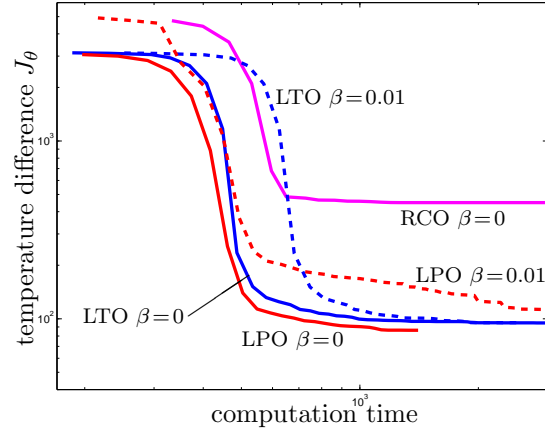

Figure 24: Efficiency in Scenario I

Figure 25: Efficiency in Scenario II

In Figures 24 and 25, we present the computation time versus the obtained temperature difference J_θ given in (4) to demonstrate the efficiency of the discussed approaches. The slow decreasing of the temperature difference at the beginning of the gradient iterations is caused from the initially small step size $\lambda = 10^{-4}$ in the line search and its moderate increasing during the gradient iterations. Furthermore, the slow decreasing of the temperature difference at the end lies in the nature of the gradient method. One can see that the *laser power and laser position optimization* (LPO) approach with $\beta = 0$ is the most efficient. However, as shown in Examples 3.1 and 3.2, the obtained laser track is not realizable by industrial robots guiding the laser. Also, smoothing the laser track does not deliver a suitable laser track for nonsmooth target curves. On the other hand, the *laser power and laser track optimization* (LTO) approach with smoothing the laser acting curve by use of $\beta > 0$ is also efficient, since it satisfies the production goal very well and yields a laser track which, depending on the parameter β, is suitable for industrial robots. Furthermore, Examples 3.5 and 3.6 shows that the efficiency and, in particular, the obtained optimization results of the *laser power and robot control optimization* (RCO) approach are not acceptable.

Summarizing, the LPO approach in Section 3.2 is suitable for smooth target curves, since the laser position is restricted to the target curve. The penalty parameter β allows a smoothing of the laser track along the target curve, see Example 3.1. On the other hand, this approach is not suitable for nonsmooth target curves because of occurring large acceleration of the laser acting point passing some discontinuities like corners, see Example 3.2. The LTO approach in Section 3.3 is suitable for arbitrary continuous target curves, since the laser position can be chosen on the surface. The

relation to a robot guiding the laser is possible by use of the acceleration penalty term, see Examples 3.3 and 3.4. Finally, the gradient method used in the RCO approach see Section 3.4, converges very slowly, since the model reacts too sensitive to perturbations/changes of the robot control, see Examples 3.5 and 3.6.

As a consequence of the obtained optimization results for the examples presented in this paper and further numerical tests, we suggest a hybrid optimization approach, i.e., the *laser power and laser track optimization* followed by a standard *path planning approach*, e.g., [13, 14, 22], to compute the according robot control.

References

[1] F.M.L. Amirouche. *Computional Methods in Multibody Dynamics*. Prentice Hall, Englewood Cliffs, Chicago, 1992.

[2] J.C. Butcher. *Numerical methods for ordinary differential equations*. John Wiley & Sons Ltd., Chichester, 2003.

[3] F.L. Chernousko. Optimization in control of robots. In R. Bulirsch and D. Kraft, editors, *Computational Optimal Control*, International Series of Numerical Mathematics 115, pages 367–382. Birkhäuser, Basel, 1994.

[4] R. Courant and D. Hilbert. *Methoden der Mathematischen Physik*. Springer-Verlag, Berlin, 4th edition, 1993.

[5] A. Eichberger. *Simulation von Mehrkörpersystemen auf parallelen Rechnerarchitekturen*. Number 332 in Fortschritt-Berichte VDI, Reihe 8: Meß-, Steuerungs- und Regelungstechnik. VDI-Verlag Düsseldorf, 1993.

[6] H.O. Fattorini. *Infinite-dimensional optimization and control theory*, volume 62 of *Encyclopedia of Mathematics and its Applications*. Cambridge University Press, Cambridge, 1999.

[7] J. Fuhrmann and D. Hömberg. Numerical simulation of surface hardening of steel. *International Journal of Numerical Methods for Heat and Fluid Flow*, 9:705–724, 1999.

[8] C.W. Gear. *Numerical Initial Value Problems in Ordinary Differential Equations*. Prentice-Hall, Englewood Cliffs, New Jersey, 1971.

[9] E. Hairer and G. Wanner. *Solving Ordinary Differential Equations II - Stiff and Differential-Algebraic Problems*. Springer-Verlag, Berlin, 2nd edition, 1996.

[10] D. Hömberg and D. Kern. The heat treatment of steel — a mathematical control problem. *Materialwiss. Werkstofftech.*, 40:438–442, 2009.

[11] D. Hömberg and S. Volkwein. Control of laser surface hardening by a reduced-order approach using proper orthogonal decomposition. *Math. Comput. Modelling*, 38:1003–1028, 2003.

[12] D. Hömberg and W. Weiss. PID-control of laser surface hardening of steel. *IEEE Transactions on Control Systems Technology*, 14:896–904, 2006.

[13] J.C. Latombe. *Robot Motion Planning*. Kluwer Academic Publishers, Norwell, Mass., 1991.

[14] S.M. Lavalle and S.A. Hutchinson. Optimal motion planning for multiple robots having independent goals. *IEEE Trans. on Robotics and Automation*, 14:912–925, 1996.

[15] M. Lehner. Entwicklung eines Simulationsmoduls zur Analyse von Mehrkörpersystemen in einem übergeordneten CAE-System. Diplomarbeit, Lehrstuhl für Mechanik der Universität Erlangen-Nürnberg, 2002.

[16] R.E. Roberson and R. Schwertassek. *Dynamics of multibody systems*. Springer-Verlag, Berlin, Germany, 1988.

[17] D. Rüdiger and A. Kneschke. *Technische Mechanik - Kinematik, Kinetik*, volume 3. Teubner Verlag, Leipzig, 1964.

[18] W. Rulka. Effiziente Simulation der Dynamik mechatronischer Systeme für industrielle Anwendungen. Technical Report IB 532–01–06, DLR German Aerospace Center, Institute of Aeroelasticity, Vehicle System Dynamics Group, 2001.

[19] W.O. Schiehlen. *Multibody System Handbook*. Springer-Verlag, Berlin, 1990.

[20] A. Steinbrecher. *Numerical Solution of Quasi-Linear Differential-Algebraic Equations and Industrial Simulation of Multibody Systems*. PhD thesis, Technische Universität Berlin, 2006.

[21] A. Steinbrecher. GEOMS: A new software package for the numerical simulation of multibody systems. In *Proceedings of EUROSIM/UKSim 2008, Cambridge, April 01-03, 2008*, pages 643–648. IEEE Computer Society, Los Alamitos, CA, USA, 2008.

[22] P. Svestka and M.H. Overmars. Coordinated path planning for multiple robots. *Robotics and Autonomous Systems*, 23:125–152, 1998.

[23] O. von Stryk and M. Schlemmer. Optimal control of the industrial robot Manutec r3. In R. Bulirsch and D. Kraft, editors, *Computational Optimal Control*, International Series of Numerical Mathematics 115, pages 367–382. Birkhäuser, Basel, 1994.

A   Laser Power and Robot Motion Optimization

In this approach, we consider again the coupled system consisting of the heat equation (5) coupled with the second-order equations of motion (9) with $B = I$ for the robot. Furthermore, let us use the position p of the robot as optimization variable in addition to the laser power u_l. With $g(p, \dot{p}, \ddot{p}, t) = \ddot{p} - f(p, \dot{p}, t)$ the robot control u_r is determined as

$$u_r = g(p, \dot{p}, \ddot{p}, t). \tag{23}$$

Let an admissible set $\mathcal{U}_{ad}^p$ for p be defined as

$$\mathcal{U}_{ad}^p \{ p \in C^4(\mathbb{I}, \mathbb{R}^n) \mid u_r(0) = u_r(T) = 0, \ \dot{u}_r(0) = \dot{u}_r(T) = 0 \}.. \tag{24}$$

Our goal is now to find an optimal laser power $u_l \in \mathcal{U}_{ad}^{u_l}$ and an optimal robot position $p \in \mathcal{U}_{ad}^p$ minimizing

$$J(u_l, p) = J_\theta + J_R = J_\theta + +\frac{\alpha}{2} \int\limits_0^T u_l(t)^2 \, \mathrm{d}t + \frac{\beta}{2} \int\limits_0^T \|g(p(t), \dot{p}(t), \ddot{p}(t), t)\|_2^2 \, \mathrm{d}t \tag{25}$$

subject to the heat equation (5). Here, the laser track is a function of p, i.e, $l = l(p)$ With the Lagrange multipliers μ_θ, the Lagrange function is given by

$$
\begin{aligned}
L(\theta, p, u_l, \mu_\theta) \ = \ & \frac{1}{2} \int\limits_0^T \int\limits_\Omega \omega(\theta - \theta^*)^2 \, \mathrm{d}x \, \mathrm{d}t + \frac{\alpha}{2} \int\limits_0^T u_l^2 \, \mathrm{d}t + \frac{\beta}{2} \int\limits_0^T \|g(p, \dot{p}, \ddot{p}, t)\|_2^2 \, \mathrm{d}t \\
& - \int\limits_0^T \int\limits_\Omega \mu_\theta (\rho c \tfrac{\partial}{\partial t} \theta - \kappa \Delta \theta - F) \, \mathrm{d}x \, \mathrm{d}t - \int\limits_0^T \int\limits_\Gamma \mu_\theta \tfrac{\partial}{\partial \nu} \theta \, \mathrm{d}x \, \mathrm{d}t.
\end{aligned}
$$

Necessary conditions for a stationary point $(\hat{\theta}, \hat{p}, \hat{u}_l)$ to be optimal is that the relations

$$\frac{\partial}{\partial \theta} L h_\theta = 0 \qquad \text{on} \quad \Omega \times \mathbb{I}, \tag{26a}$$

$$h_\theta(x, 0) = 0 \qquad \text{on} \quad \Omega, \tag{26b}$$

$$\frac{\partial}{\partial \nu} h_\theta(x, t) = 0 \qquad \text{on} \quad \Gamma \times \mathbb{I}, \tag{26c}$$

$$\frac{\partial}{\partial p} L(p - \hat{p}) \geq 0, \tag{26d}$$

$$\frac{\partial}{\partial u_l} L(u_l - \hat{u}_l) \geq 0 \tag{26e}$$

are satisfied for all suitable test functions h_θ as well as for $p \in \mathcal{U}_{ad}^p$ and $u_l \in \mathcal{U}_{ad}^{u_l}$. The conditions (26a)-(26c) and (26e) are the same as in Section 3.2 and, therefore,

they correspond to (17b) and (17c) with (17e).
Using integration by parts, we get

$$\frac{\partial}{\partial p}L(p-\hat{p}) \;=\; \beta\int\limits_0^T g^T\tfrac{\partial}{\partial p}g(p-\hat{p})\,\mathrm{d}t + \beta\int\limits_0^T g^T\tfrac{\partial}{\partial\dot{p}}g(\dot{p}-\dot{\hat{p}})\,\mathrm{d}t + \beta\int\limits_0^T g^T\tfrac{\partial}{\partial\ddot{p}}g(\ddot{p}-\ddot{\hat{p}})\,\mathrm{d}t$$

$$+ \int\limits_0^T\int\limits_\Omega \mu_\theta\tfrac{\partial}{\partial l}F\tfrac{\partial}{\partial p}l(p-\hat{p})\,\mathrm{d}x\,\mathrm{d}t$$

$$=\; \beta\int\limits_0^T g^T\tfrac{\partial}{\partial p}g(p-\hat{p})\,\mathrm{d}t + \beta g^T\tfrac{\partial}{\partial\dot{p}}g(p-\hat{p})|_0^T - \beta\int\limits_0^T \tfrac{\mathrm{d}}{\mathrm{d}t}(g^T\tfrac{\partial}{\partial\dot{p}}g)(p-\hat{p})\,\mathrm{d}t$$

$$+\beta g^T\tfrac{\partial}{\partial\ddot{p}}g(\dot{p}-\dot{\hat{p}})|_0^T - \beta\tfrac{\mathrm{d}}{\mathrm{d}t}(g^T\tfrac{\partial}{\partial\ddot{p}}g)(p-\hat{p})|_0^T + \beta\int\limits_0^T \tfrac{\mathrm{d}^2}{\mathrm{d}t^2}(g^T\tfrac{\partial}{\partial\ddot{p}}g)(p-\hat{p})\,\mathrm{d}t$$

$$+ \int\limits_0^T\int\limits_\Omega \mu_\theta\tfrac{\partial}{\partial l}F\tfrac{\partial}{\partial p}l(p-\hat{p})\,\mathrm{d}x\,\mathrm{d}t.$$

It follows from (23) and (24) that $g(\hat{p}(\tau),\dot{\hat{p}}(\tau),\ddot{\hat{p}}(\tau),\tau)=0$ and $\tfrac{\mathrm{d}}{\mathrm{d}t}g(\hat{p}(\tau),\dot{\hat{p}}(\tau),\ddot{\hat{p}}(\tau),\tau)=0$ for $\tau\in\{0,T\}$. Note that $\tfrac{\partial}{\partial\ddot{p}}g=I$. Using (26d) we get

$$\int\limits_0^T\left(\beta\big(g^T\tfrac{\partial}{\partial p}g - \tfrac{\mathrm{d}}{\mathrm{d}t}(g^T\tfrac{\partial}{\partial\dot{p}}g) + \tfrac{\mathrm{d}^2}{\mathrm{d}t^2}(g^T\tfrac{\partial}{\partial\ddot{p}}g)\big) + \int\limits_\Omega \mu_\theta\tfrac{\partial}{\partial l}F\tfrac{\partial}{\partial p}l\,\mathrm{d}x\right)(p-\hat{p})\,\mathrm{d}t \geq 0$$

for all $p\in\mathcal{U}_{ad}^p$. Then the first-order optimality conditions are given by

$$\rho c\tfrac{\partial}{\partial t}\hat{\theta} - \kappa\Delta\hat{\theta} = F \qquad\qquad \text{on}\quad \Omega\times\mathbb{I}, \qquad\qquad (27a)$$
$$\hat{\theta}(x,0) = \theta_0 \qquad\qquad \text{on}\quad \Omega,$$
$$\tfrac{\partial}{\partial\nu}\hat{\theta}(x,t) = 0 \qquad\qquad \text{on}\quad \Gamma\times\mathbb{I},$$

$$-\rho c\tfrac{\partial}{\partial t}\mu_\theta - \kappa\Delta\mu_\theta = \omega^2(\hat{\theta}-\theta^*) \qquad\qquad \text{on}\quad \Omega\times\mathbb{I}, \qquad\qquad (27b)$$
$$\mu_\theta(x,T) = 0 \qquad\qquad \text{on}\quad \Omega,$$
$$\tfrac{\partial}{\partial\nu}\mu_\theta(x,t) = 0 \qquad\qquad \text{on}\quad \Gamma\times\mathbb{I},$$

$$\int\limits_0^T G_{u_l}(u_l-\hat{u}_l)\,\mathrm{d}t \geq 0 \qquad\qquad \text{for all}\quad u_l\in\mathcal{U}_{ad}^{u_l}, \qquad\qquad (27c)$$

$$\int\limits_0^T G_p(p-\hat{p})\,\mathrm{d}t \geq 0 \qquad\qquad \text{for all}\quad p\in\mathcal{U}_{ad}^p, \qquad\qquad (27d)$$

where

$$G_{u_l} = \alpha u_l + \int_\Omega \mu_\theta \frac{\partial}{\partial u_l} F \, \mathrm{d}x, \tag{27e}$$

$$G_p = \beta \left(g^T \frac{\partial}{\partial p} g - \frac{\mathrm{d}}{\mathrm{d}t} (g^T \frac{\partial}{\partial \dot{p}} g) + \frac{\mathrm{d}^2}{\mathrm{d}t^2} (g^T \frac{\partial}{\partial \ddot{p}} g) \right) + \int_\Omega \mu_\theta \frac{\partial}{\partial l} F \frac{\partial}{\partial p} l \, \mathrm{d}x. \tag{27f}$$

Due to the high order of derivatives in (27f) the approach of laser power and robot motion optimization is not feasible from a numerical point of view and only included for the sake of completeness.